Solution-produced copper iodide thin films for photosensor and for vertical thermoelectric nanogenerator, which uses a spontaneous temperature gradient

N. P. Klochko[1] · K. S. Klepikova[1] · V. R. Kopach[1] · D. O. Zhadan[1] · V. V. Starikov[1] · D. S. Sofronov[2,3] · I. V. Khrypunova[1] · S. I. Petrushenko[4] · S. V. Dukarov[4] · V. M. Lyubov[1] · M. V. Kirichenko[1] · S. P. Bigas[1] · A. L. Khrypunova[1]

Abstract

The article presents a new design of vertical thermoelectric nanogenerator (TENG) on the base of thin-film CuI/FTO composition with ohmic Cr/Cu contacts, which combines the functions of UV–Visible photosensor. Its functioning as the TENG carried out due to the spontaneous temperature gradient approximately 7 K, which occurs under the uniform heating of the entire device at temperature 30 °C. The open circuit voltage of TENG test sample is $V_{oc} = 0.09$ mV and maximum output power is $P_{max} = 0.4$ nW at temperature 50 °C. UV–Visible photosensor based on Cu/Cr/CuI/FTO/Cr/Cu composition possess high values of photocurrents I_{ph} under illumination, which eliminates necessity of amplification of the photosensor signal. The photoresponse and reset times of the photosensor are $\tau_p \approx 30–100$ s and $\tau_r \approx 20–100$ s, respectively. The explanation of the possibility of using CuI thin films, solution-produced by the affordable successive ionic layer adsorption and reaction (SILAR) method as both thermoelectric and photosensitive material is based on the studying of surface morphology, crystal structure, chemical composition and optical properties.

1 Introduction

New approaches to the harvesting and transforming into electricity the waste energy from the living environment instead of the conventional battery to power small electronic devices and systems are attracting increasing attention [1–9]. In particular, wireless power supply is a critical issue in realizing the internet of things (IoT), in which sensing, data collection, and communication would be performed using a trillion-sensor network [2, 5]. In accordance with [5, 8], there are four forms of energy sources available for harvesting from the environment, namely, visible light, radio frequency electromagnetic radiation, motion, and heat flow. As the sizes of the devices shrunk to the nanoscale, the power consumption also decreases to the nW level. Therefore, a thermoelectric energy scavenging using a network of thermoelectric nanogenerators (TENGs) could be a viable source of power for autonomous wireless devices through transforming of little heat flow into electricity [1–7]. However, the key challenge is to create a significant temperature gradient (ΔT) across the device without a spatial temperature difference in the environment [3, 5], because ΔT is a driving force of the TENG.

In TENG described in [2], which elaborated using a microelectromechanical system process, the temperature gradient can be created, for example, by a circulating air flow or infrared (IR) radiation, between suspended silicon nitride membrane and bulk silicon frame. Since membrane has a negligible mass, its temperature is free to fluctuate contrary to the bulk silicon frame. According to [2], the power generated by an individual membrane by using air flow under near-room temperature is around 0.3 nW for $\Delta T \approx 8$ K. However, the microfabrication process used in [2] to make this TENG requires appropriate expensive equipment.

✉ K. S. Klepikova
catherinakle@gmail.com

1   Department of Materials for Electronics and Solar Cells, National Technical University "Kharkiv Polytechnic Institute", 2, Kirpichov St, Kharkiv 61002, Ukraine

2   Institute for Single Crystals, NAS of Ukraine, 60, Nauky Ave, Kharkiv 61001, Ukraine

3   State Scientific Institution « Institute for Single Crystals » of NAS of Ukraine, 60, Nauky Ave, Kharkiv 61001, Ukraine

4   Kharkiv National University named after V. N. Karazin, 4, Svobody Square, Kharkiv 61022, Ukraine

Authors [3] presented thin-film nanogenerator for the harvesting environmental IR radiation. This nanogenerator was obtained through deposition from solutions of nanocomposite films contained hydrothermally synthesized molybdenum disulfide (MoS_2) nanoclusters and tellurium (Te) nanowires. In this nanogenerator of planar (in-plane) type, one of the Ag electrodes was coated by nanocomposite film on the base of MoS_2 used as photothermal material with higher IR absorbance. Under heating, MoS_2 nanoclusters as a part of MoS_2/polyurethane nanocomposite film absorb infrared radiation and thus form in TENG the gradient ΔT across thermoelectric nanocomposite layer with Te nanowires. The difference between two electrodes (hot Ag electrode coated by MoS_2/polyurethane film and cold naked Ag electrode) connecting the ends of a nanocomposite layer with Te nanowires can generate electricity, when whole nanogenerator submitted to a heat source, that is, without a spatial temperature gradient.

An interesting and relevant approach is the creation of semi-transparent thermoelectric materials based on available and non-toxic wide band gap compounds [10–12], in contrast to the designs of thermoelectric generators developed in [2, 3]. This approach opens up prospects for the further development of semi-transparent electronics in the field of developing smart windows or screens, semi-transparent optoelectronic devices, etc. For example, in [9] we developed and successfully tested a new design of semi-transparent vertical (out-of-plane) type TENG using an array of vertically aligned ZnO nanorods electrodeposited on transparent conducting fluorine doped tin oxide (FTO) substrate. An operation of this TENG caused by the temperature gradient between tops of ZnO nanorods and uncoated FTO that spontaneously created due to heat flow from solar near-infrared (NIR) light and/or mid-infrared (MIR) radiation from the ambient warm. The obtained by TENG in [9] output power at near-room temperature without a spatial temperature gradient in the environment is ~ 62 pW/cm^2. The network of such TENGs can serve as a source of electricity sufficient to make sensors wholly autonomous in energy, according to the data [2, 13], by the harvesting NIR energy of sunlight and heat from ambient.

In [9] arrays of ZnO nanorods were obtained on FTO substrates by pulsed electrochemical deposition method, which is suitable for large surfaces and suggests low capital expenditure based on simple process equipment. However, low cost affordable Successive Ionic Layer Adsorption and Reaction (SILAR) method is even easier and more adapted for mass production [14]. Moreover, as we showed earlier [15, 16], copper iodide (CuI) films produced by SILAR have promising thermoelectric properties. We used in this work SILAR technique for the creation of vertical TENG with design similar to [9]. Some disadvantage of the proposed TENG design is the opaque Cr/Cu metal frontal electrode, which is then supposed to be replaced to increase

transparency with a transparent conductive oxide film. In addition, as it turned out from our experiments, the same CuI/FTO based TENG design can be used as a photosensor of photoconductor type, if between its electrodes will be applied a voltage from an external source. In this way, it is possible to create a two-function device that is an interesting modern approach.

Thus, in this paper, we investigate a new design of TENG created using CuI/FTO compositions with solution-produced copper iodide thin films. By means studying surface morphology, crystal structure, chemical composition and optical properties of CuI films, we explain the spontaneous occurrence of the temperature gradient and the functioning of the above TENG as a whole. Additionally, on the base of study of the CuI/FTO photosensitivity to ultraviolet (UV) and visible light we demonstrate for the first time the possibility of using the TENG design as efficient UV–Visible photosensor of photoconductor type.

2 Experimental procedures

In this study, we used 2×3 cm FTO glass substrates (TEC 7 from Pilkington NSG TEC™). Deposition of CuI thin films on FTO via SILAR method was carried out using an aqueous solution containing 0.1 M $CuSO_4$ and 0.1 M $Na_2S_2O_3$ as a cationic precursor. FTO substrates were immersed in about three-quarters or on half of their square into the cationic precursor for 20 s. Then, the substrate washed with distilled water for 10 s. For the reaction of the firmly adsorbed Cu^+ ions on the FTO surface with I^- ions to obtain CuI monolayers, the substrates were then immersed for 20 s into aqueous NaI solution (anionic precursor), which concentration was 0.05, 0.075 or 0.1 M. After that, FTO substrates washed with distilled water for 10 s. The listed procedure was one SILAR cycle of CuI film deposition. Such SILAR cycles were repeated 40−60 times. Thereafter, the deposited CuI film on FTO washed with distilled water and dried in an air stream. The thickness of the CuI films t in the 0.1−1.2 μm range was determined gravimetrically as in [14], taking for a calculation the bulk CuI density 5.67 g/cm^3. The copper iodide films that deposited on the opposite side of the FTO substrates removed by wiping with 20% sulfuric acid solution. In appearance and as seen in Fig. 5, the resulting CuI films are semi-transparent and well bonded to the FTO substrates.

Morphology of CuI films deposited on FTO substrate via SILAR method was observed by scanning electron microscopy (SEM) in a secondary electron mode. The SEM instrument "Tescan Vega 3 LMH" operated at an accelerating voltage 30 kV without the use of additional conductive coatings. Chemical analysis of this CuI film in the CuI/FTO sample, and also of FTO substrate was

carried out by X-ray fluorescence (XRF) microanalysis using an energy dispersive spectrometry (EDS) system "Bruker XFlash 5010". Energy dispersion spectra were taken from the 50×50 µm film area. Quantification of the spectrum was carried out in the self-calibrating detector mode.

Optical properties of CuI films in UV–Visible-near IR range (at wavelengths (λ) 300–1100 nm) studied with an "SF-2000" spectrophotometer equipped with "SFO-2000" specular and diffuse reflection attachment. FTO substrates were used as control samples when optical transmission spectra $T_o(\lambda)$ of CuI/FTO samples were recorded. Optical band gaps E_g of the CuI films were determined from their absorption coefficients (α) calculated as described in [17]:

$$\alpha = 1/t \cdot \ln(1/T_o). \tag{1}$$

Then, the optical band gaps E_g were obtained via the following equation [17]:

$$(\alpha \cdot h\nu)^2 = A \cdot (h\nu - E_g), \tag{2}$$

where A is a factor that depends on the transition probability and can be assumed to be constant within the optical frequency range, and $h\nu$ denotes the photon energy. The E_g value obtained graphically through an extrapolation of the linear portion of the $(\alpha \cdot h\nu)^2$ dependence on $h\nu$.

The Urbach energy (E_o), that originates from the optical transitions caused by subband gap photons, which are mainly due to the presence of point defects in the CuI material was determined, in accordance with [17], by equation:

$$a = \alpha_o \cdot \exp(h\nu/E_o), \tag{3}$$

where α_o is a constant, which corresponds to optical absorption coefficient at the absorption onset. To wit, α_o is a coordinate of the convergence point of the Urbach "tail", i.e. $\alpha = \alpha_o$, when $h\nu = 0$. Therefore, the structural disorder of the CuI film was assessed from the E_o determined by fitting the linear portions of ln(α) versus $h\nu$ near $h\nu \approx E_g$ as the slope cotangent.

The light scattering in the CuI film, haze factor (Hf), was calculated as the ratio of the diffuse reflectance R_d to the total reflectance R, that is $Hf = R_d/R$.

Infrared transmission spectra for FTO substrate and for CuI/FTO samples with CuI films deposited via SILAR were obtained using Fourier transform infrared spectroscopy (FTIR) method with a Fourier spectrophotometer SPECTRUM ONE (PerkinElmer) in the 400–4000 cm^{-1} range (at wavelengths from 2.5 to 25 µm) and at a resolution of 1 cm^{-1} at room temperature. In addition, for IR studies by means of FTIR spectroscopy we used tablets with potassium bromide (KBr) filler. For this, CuI film was scraped off the FTO substrate surface with a scalpel, and then mixed with KBr, triturated and tableted.

To analyze phase compositions and structural parameters of the CuI films, we recorded X-ray diffraction patterns by a "DRON-4" diffractometer as in [16] (XRD method). The microstrains ε in the nanocrystalline CuI films $\varepsilon = \Delta d/d$ (where d which is named here d-spacing is the crystal interplanar spacing according to the reference database JCPDS, and Δd is the difference between the corresponding experimental and reference interplanar spacing) estimated by an analyzing the broadening of the X-ray diffraction peaks using the Scherrer's method [18]. The average crystallite size (D) was calculated using Scherrer's formula as in [14, 18]:

$$D = (0.9 \cdot \lambda)/(\beta \cdot \cos\theta), \tag{4}$$

where λ is X-ray wavelength; $\beta = (B-b)$, when B is the observed Full Width at Half Maximum (FWHM), and b is the broadening in the peak due to the instrument in radians, θ denotes the Bragg's angle of the X-ray diffraction peaks (111) and (220). Dislocation density was evaluated as $1/D^2$ according to [19]. Texture quality of CuI films estimated by the Harris method [9, 20] using values of pole density $P_{(hkl)}$, which determines an axis of the crystal plane that is oriented normally to the surface.

To analyze a photosensitivity of the copper iodide films towards UV and visible light, we made CuI/FTO based test samples, on which ohmic chromium/copper (Cr/Cu) banded contacts applied through vacuum deposition on the naked FTO and on the CuI surfaces, as presented in Fig. 1. The same test samples we research here as a new design of vertical TENG, which schematic illustration and two setups for their characterization are also shown in Fig. 1. Figure 1a on the right shows a schematic design of our TENG consisted of FTO plate, which on half its square covered by CuI film, with two banded Cr/Cu contacts. In the process of the TENG/photosensor test sample creating, vacuum deposition of Cr and Cu carried out at 25° angle to the substrates on limited areas of FTO and CuI through a shadow mask in order to avoid a shunting. Then, conductive adhesive with silver filler applied to the Cr/Cu surface for providing galvanic contacts with copper wires.

The proposed design of the TENG/photosensor provides dual functionality of the device due to the spontaneous occurrence of temperature gradient between the two contacts on account of the more intense absorption of IR radiation by a CuI film compared to FTO. Besides using of FTO due to its transparency in the UV and visible radiation range provides greater absorption of the incident radiation by a CuI film, since the UV–Visible photodetector is illuminated through the FTO side. Reliable operation of the TENG/photosensor is ensured by the thermally and mechanically stable ohmic Cr/Cu contacts under operating conditions, in particular due to the physical properties of chromium.
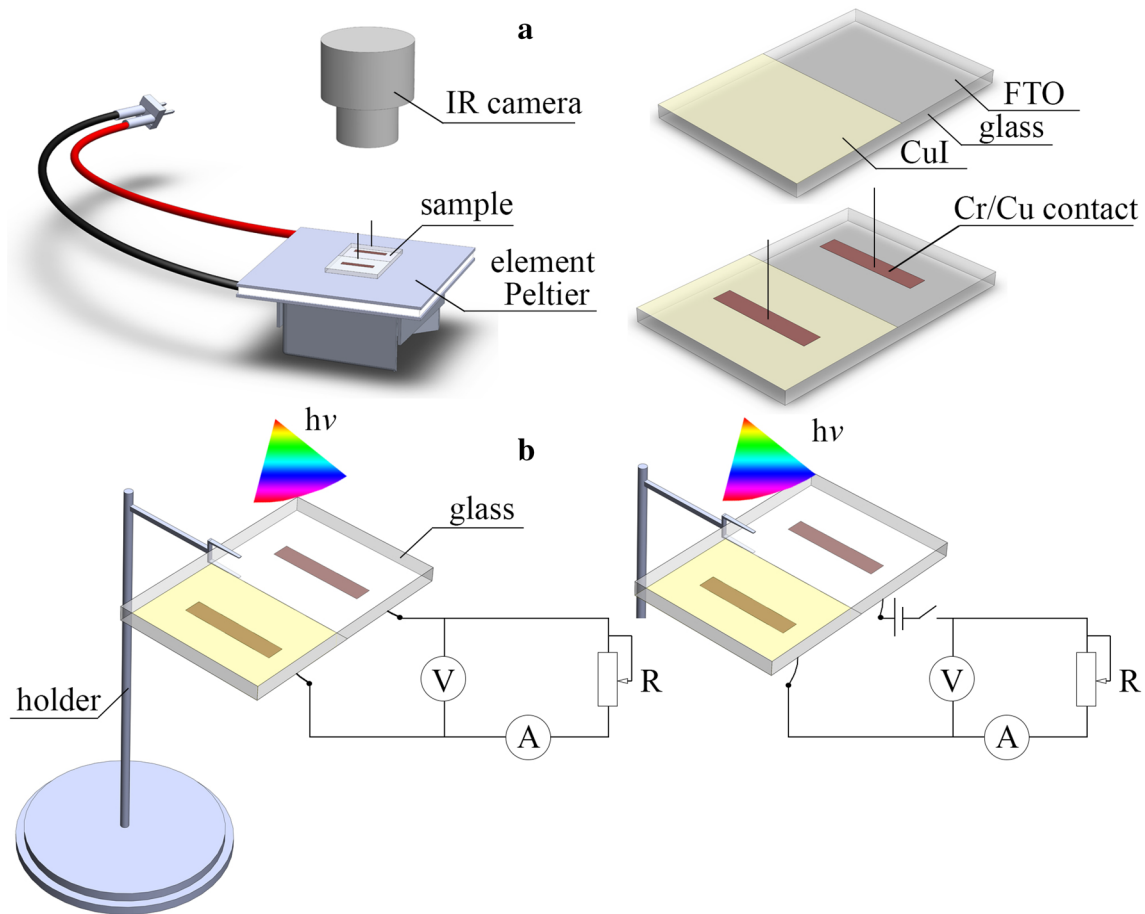
Fig. 1 Schematic illustration of the developed thin-film vertical TENG/photosensor test sample on the base of CuI/FTO and two set-ups for its characterization. **a**—Setup for a measuring of temperature distribution over the heated TENG area (on the left) and schematic design of TENG without and with Cr/Cu contacts (on the right).

b—Setup on the left to obtain output characteristics of TENG under illumination by halogen lamp (at zero voltage bias) and setup on the right for a measuring the photosensitivity of Cu/Cr/CuI/FTO/Cr/Cu composition as UV–Visible photosensor (at bias voltage 0.5 V from DC power supply)

Temperature gradient ΔT between CuI and uncoated FTO substrate was created and investigated using hot plate of the Peltier element "TEC1-12730", on which test sample CuI/FTO without Cr/Cu contacts or test sample of the developed TENG/photosensor was located as it shown in Fig. 1a on the left. Temperature distributions over the heated area, including ΔT between CuI surface and uncoated FTO substrate, fixed and measured by an infrared camera "FLUKE Ti10".

Figure 1b shows schematic setup with a variable resistor "R" as a load for a measuring of output characteristics of TENG test sample under illumination with halogen lamp with reflector "Philips Plusline L1CT/10" in order to heat the entire device up to 50 °C. Here "V" is a voltmeter for a measuring of output voltage V_{out}; "A" denotes a microampere meter for a measuring of output current I_{out}. Note that the TENG in Fig. 1b is fixed in a holder so that the CuI film is at the bottom, and the light enters the CuI film through the FTO plate from glass side.

In order to study the photosensitivity of the created UV–Visible photosensor of photoconductor type, we measured photoresponse curves of the TENG/photosensor test samples at bias voltage 0.5 V between two Cr/Cu contacts. The test samples were illuminated with UV ($\lambda = 365$ nm), blue ($\lambda = 465$ nm), green ($\lambda = 525$ nm) or red ($\lambda = 625$ nm) light-emitting diodes having wide-angle beam divergences to ensure uniform illumination from the glass side (Fig. 1b). The intensity (power density) of the light on the TENG surface was 0.5 W/cm². Photocurrent I_{ph} was recorded during illumination of the TENG/photosensor test sample $\tau_{on} = 300$ s, after that, the light was turned off. A photosensitivity S of the photosensor was calculated as $S = I_{ph}/I_d$, where I_d is dark current. In accordance with [21], the photoresponse time τ_p of the test sample was determined as the time required to achieve 63% of the maximum photocurrent I_{ph} after the start of the illumination. The reset time τ_r was defined, according to [21], as the elapsed time to reach the

37% of the maximum photocurrent after the switching off the light.

3 Results and discussion

Figure 2 shows SEM image of CuI film deposited on FTO substrate via SILAR as compared with SEM image of uncoated FTO substrate. Obviously, such network-like fibrous CuI structure with a huge specific surface area must provide a high adsorption of the components of ambient air, primarily atmospheric gases and water vapor. On the contrary, the surface of FTO is dense and smooth, therefore, there are much less adsorption centers on it.

According to the XRF data in Fig. 3 and Table 1, the copper iodide film is enriched with iodine. Probably, such chemical composition corresponds to the presence of a large number of copper vacancies in the CuI film, which are point acceptor centers causing a high electrical conductivity of this material. Tin in both XRF spectra are components of FTO substrate. In accordance with [22], the appearance of O and C, might be attributed to H_2O, O_2 and CO_2 adsorbed on the surface of the CuI crystals in air. Thus, the excess oxygen content in the XRF spectrum of CuI/FTO in Fig. 3 and Table 1 can be explained by the adsorption of water and oxygen on the large specific surface of CuI. In addition, the presence of carbon can be evidence of unavoidable pollution with organic matter.

Besides, it is seen ~ 4 at. % of sulfur in XRF spectrum of CuI. As we noted earlier [16], the presence of sulfur is the distinctive feature of CuI films obtained via the SILAR technique. Probably, the source of S is a chemically
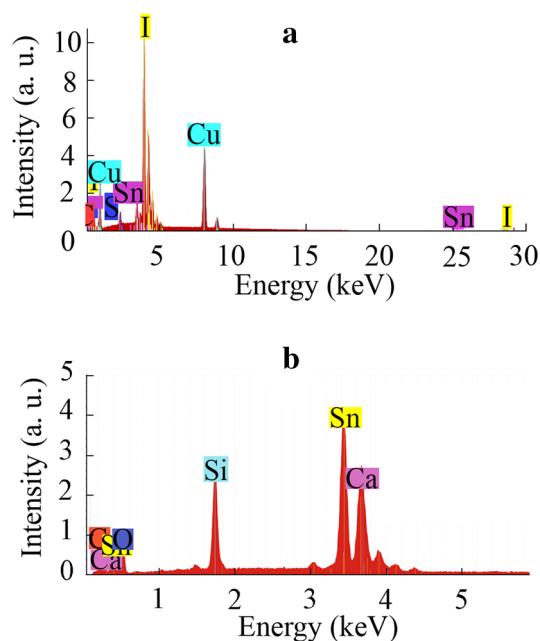

Fig. 3 Chemical composition of CuI/FTO sample with 1.2 μm thick CuI film deposited on FTO substrate via SILAR method using 0.1 M NaI anionic precursor (**a**) as compared with uncoated FTO substrate (**b**), according to data of their X-ray fluorescence microanalysis

unstable thiosulfate complex in the cationic precursor solution. Despite the fact, that we could not find any information in the literature, to our opinion, sulfur, which is an element of the sixth group, can form acceptor levels in the copper iodide and thus increase the electrical conductivity of the *p*-CuI films. On the other hand, an excess of sulfur
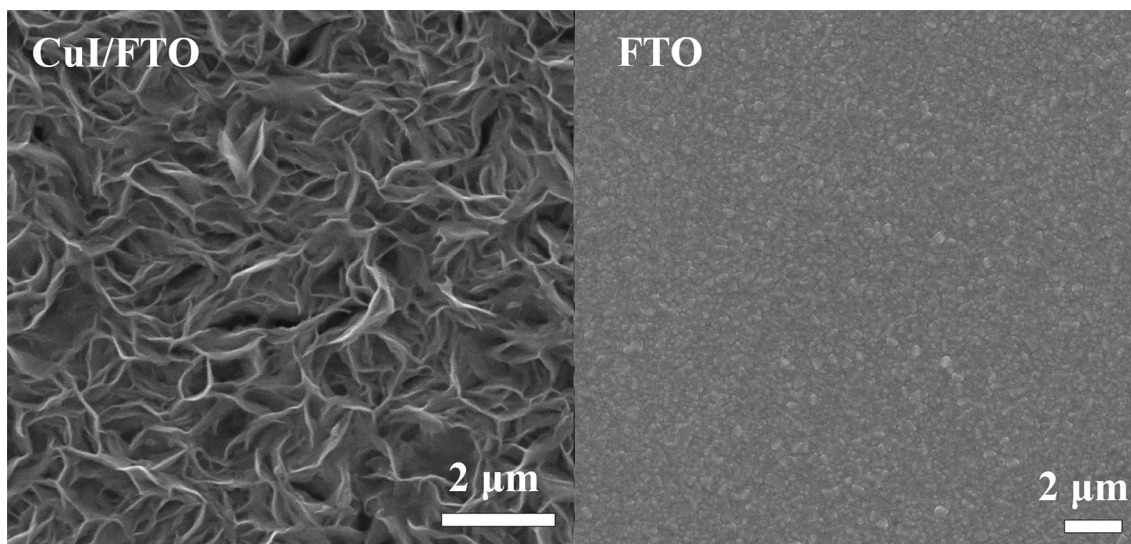

Fig. 2 Top view SEM images of 1.2 μm thick CuI film deposited on FTO substrate via SILAR method for 60 cycles using 0.1 M NaI anionic precursor (on the left) and of the uncoated FTO substrate (on the right)

Table 1 XRF data concerning chemical compositions of CuI/FTO sample with 1.2 μm thick CuI film deposited on FTO substrate via SILAR method using 0.1 M NaI anionic precursor and of uncoated FTO substrate

	Sample	
	CuI/FTO	FTO
Element	(at. %)	(at. %)
C	12	34
O	6	47
S	4	–
Cu	37	–
Sn	3	9
I	38	–
Ca	–	3
Si	–	7

in the film may cause an impurity crystalline phase of copper sulfide.

Figure 4 shows XRD patterns of three CuI/FTO samples with 0.1–0.8 μm thick CuI films deposited on FTO substrates via SILAR by using different concentrations of the anionic precursor (0.05, 0.075 and 0.1 M NaI). All diffraction patterns show the obvious presence of two crystalline phases, one of which relates to the FTO substrate, and the other one identified as the CuI film on its surface. Additional diffraction peaks in Fig. 4 that correspond to the crystal interplanar spacing $d \approx 3.63$ Å refers probably to unknown impurity crystalline phase. As it seen in Fig. 4, each XRD pattern contains several diffraction peaks, which belong to cubic Marshite copper iodide structure (zincblende, γ-CuI, JCPDS #06-0246).

Thus, all CuI films are polycrystalline. The intensity of the CuI diffraction peaks increases with the thickness of the films, which, in turn, grows with increasing concentration of the anionic precursor NaI. Calculations revealed that all CuI films are composed of very fine grains, since average crystallite size D yielded the 7–18 nm range. At that, the grain size does not depend on the CuI thickness and the SILAR mode. CuI films have slight preferred orientation in the (220) plane ($P_{(hkl)} = 1.6$ for 0.8 μm thick CuI film in Fig. 4) and high microstrains $\varepsilon \cdot = (1.0–1.5) \cdot 10^{-2}$ a.u. Dislocation density, evaluated as $1/D^2$, was $3 \cdot 10^{15}$—$2 \cdot 10^{16}$ lines/m^2.

Figure 5 shows optical properties in the UV–Vis-NIR range of the thicker CuI films (t in the 0.6–1.2 μm range) deposited via SILAR onto FTO substrates. It is evident that these CuI films are translucent due to strong diffuse reflection and light scattering, their maximum transparency T_o is not above 8.5%. The band gap E_g for direct optical transitions shown in Table 2 $E_g \approx 2.9$−3.0 eV calculated through the $(\alpha \cdot h\nu)^2$ dependence on $h\nu$ in Fig. 5 is close to the value 2.95−3.1 eV for bulk CuI at near-room temperature [23, 24]. The average Urbach energy of the CuI films deposited via SILAR $E_o \approx 0.2$–0.7 eV is quite large, probably due to their nanocrystallinity and because of the presence of large number of defects. Optical reflection spectra $R_d(\lambda)$ in Fig. 5
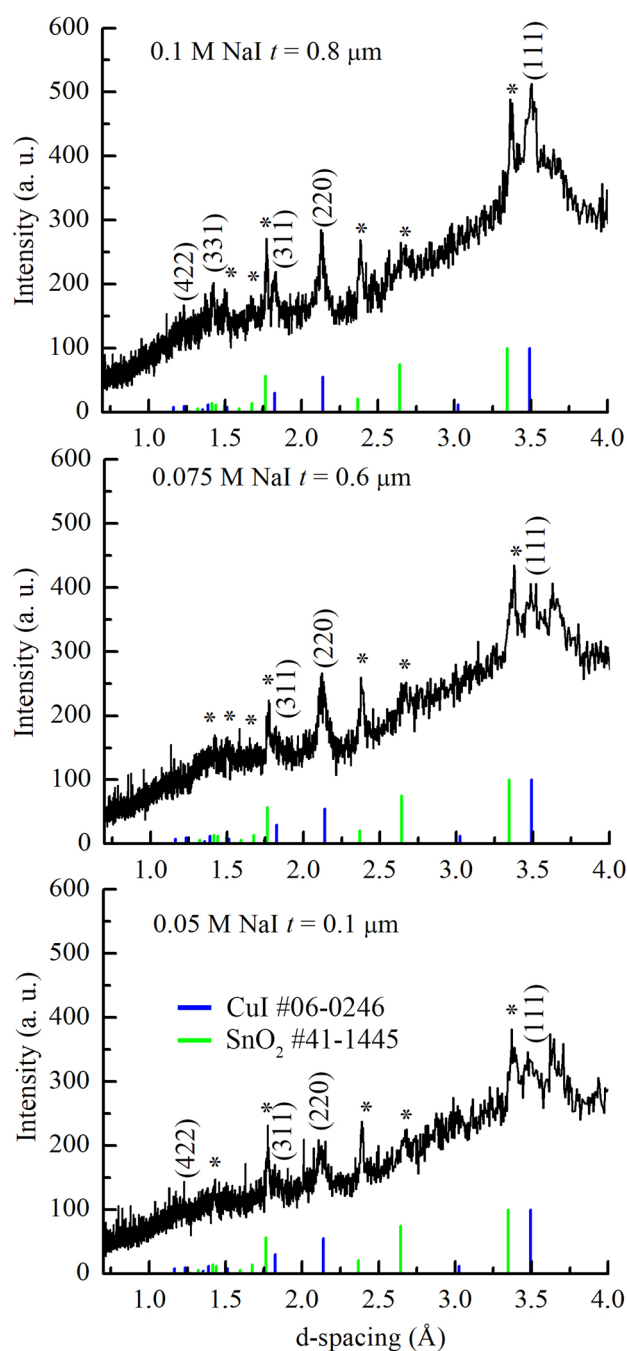

Fig. 4 XRD patterns CuI/FTO samples with 0.1–0.8 μm thick CuI films deposited on FTO substrates via SILAR by using different concentrations of the anionic precursor NaI

confirm the significant diffuse reflectance in the entire visible range, and the extremely large values of haze factor Hf correspond to the high light-scattering, which agrees well with the morphology of the CuI surface shown in Fig. 2.

Figure 6 shows infrared images with well distinguishable temperature gradients $\Delta T \approx 7$ K between surfaces of the CuI films and uncoated FTO in the CuI/FTO samples, which

Fig. 5 Optical properties in the UV–Vis-NIR range of CuI films with thickness *t*, which were deposited on FTO substrates via SILAR using different concentrations of anionic precursor NaI: **a**—transmittance spectra; **b**—graphs for the determination E_g according to Eq. (2); **c**—diffuse reflectance spectra; **d**—haze factor spectra
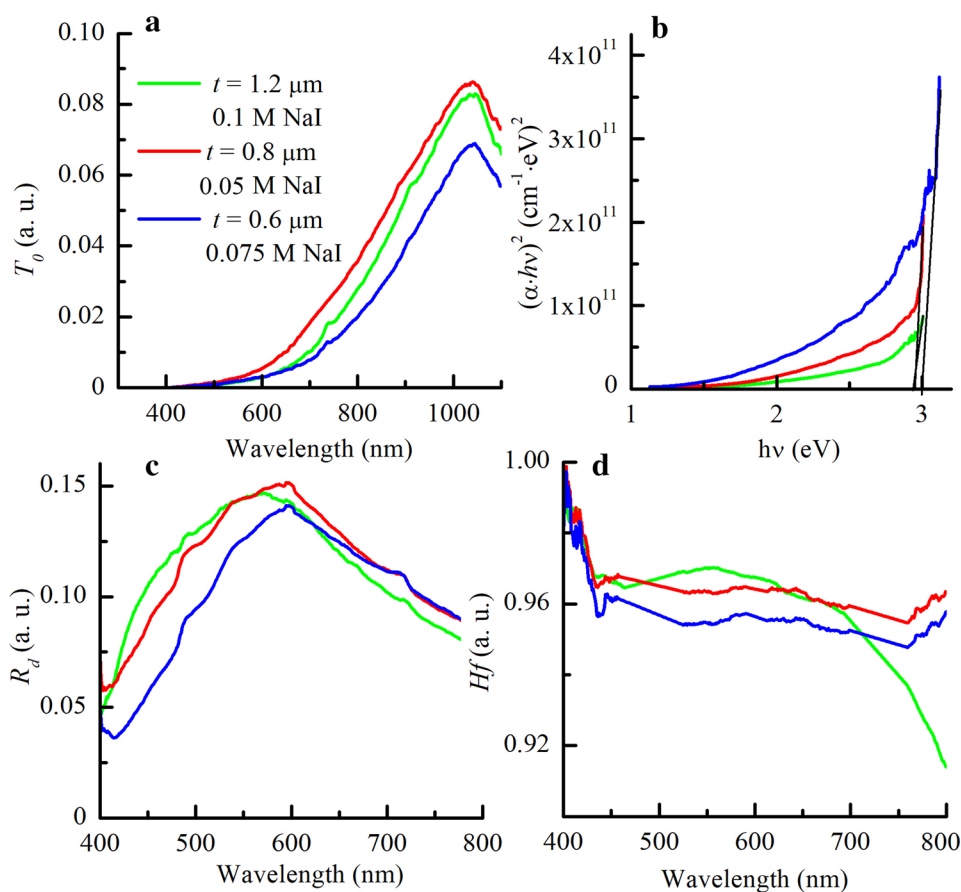

Table 2 Values for the optical band gap E_g and for the Urbach energy E_o of the CuI films with thickness *t* in CuI/FTO samples, which presented in Fig. 5

Sample		E_g (eV)	E_0 (eV)
T (MM)	NaI		
0.6	0.075 M	3.0	0.2
0.8	0.1 M	2.9	0.2
1.2	0.1 M	2.9	0.7

spontaneously created under heating the whole device up to ~30 °C using the Peltier element as shown in Fig. 1a. In addition, Fig. 6 shows also a photo of the CuI/FTO sample, lying on the Peltier element surface. It can be seen that ΔT does not depend essentially on the thickness of the CuI film and on the mode of its deposition by the SILAR method.

To explain the causes of the spontaneous temperature gradients we used infrared transmittance spectra of three CuI/FTO samples as compared to uncoated FTO substrate, which shown in Fig. 7a. It is seen in Fig. 7a, that CuI films decrease distinctly the transmittance in the short-wavelength infrared range, that is at least partly due to their absorption of heat. The corresponding three FTIR spectra of copper iodide

material scraped from these samples (Fig. 7b) allow us to find out the reason for the absorption of infrared radiation by the copper iodide films with large specific surfaces. Thus, according to the literature data, two characteristic peaks of nanocrystalline γ-CuI in FTIR spectra, which assigned to Cu-I stretching vibrations are located at 610.6 cm^{-1} [25] or at 638.92 cm^{-1} [26], and at 474 cm^{-1}, according to [25]. Our results of analysis via Fourier transform infrared spectroscopy method also demonstrated the presence of similar peaks in the all copper iodide FTIR spectra in Fig. 7b. The absorption bands with maxima at 3427 and 1632 cm^{-1} correspond to the stretching and deformation vibrations of water molecules [25–27]. These peaks may come from the surface adsorption of ambient water. Two peaks at stretching frequency of ~2900 cm^{-1}, according to [26], contribute to the C–H bond, for example due to the inevitable organic pollution of the CuI surface.

The FTIR spectra in Fig. 6b show also intense absorption in the 900–1250 cm^{-1} region with maxima at 1070 and 1019 cm^{-1}. This absorption band can be explained by traces of the solutions from which CuI films were obtained by the SILAR method. Namely, maxima at 1070 cm^{-1} is possibly attributed to the vibration of the sulfate ions SO_4^{2-}, and maxima at 1019 cm^{-1} can be associated with the oscillations of
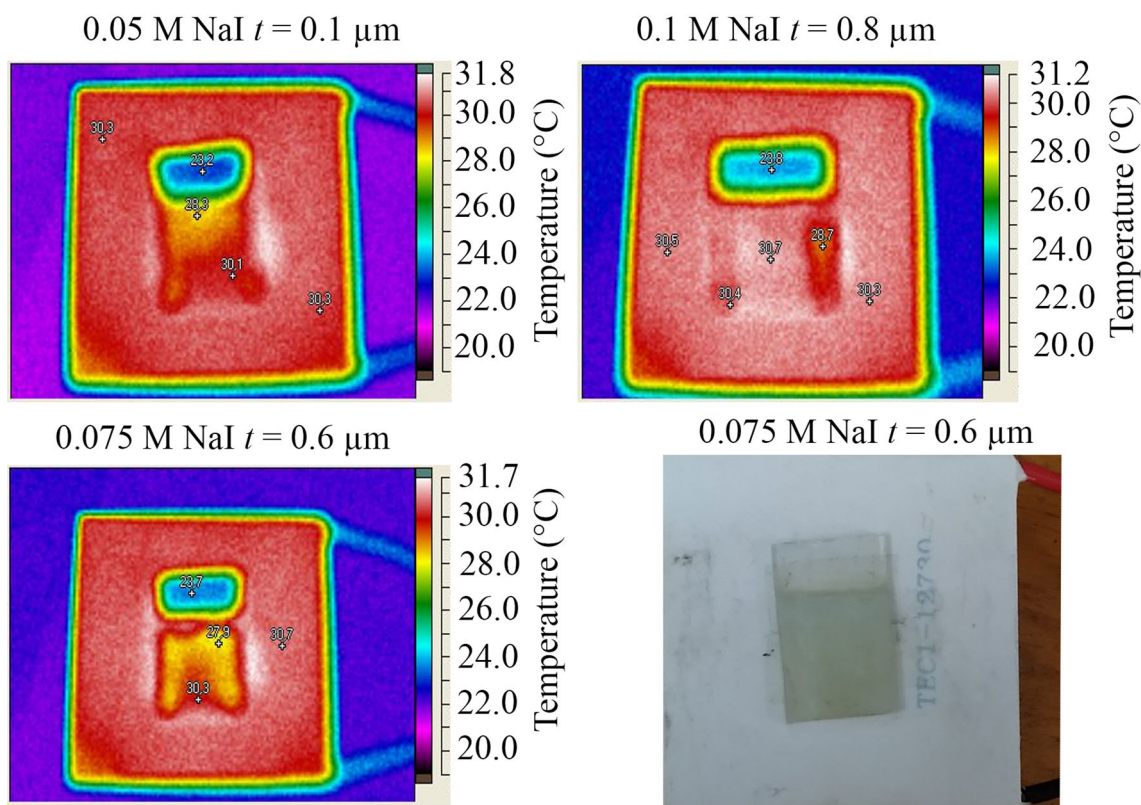
Fig. 6 Infrared images taken during heating with the Peltier element as shown in Fig. 1a for CuI/FTO samples with different CuI thicknesses t, which were deposited on FTO substrates via 40 cycles of SILAR using different concentrations of anionic precursor NaI. Photo of CuI/FTO sample with 0.6 μm thick CuI film obtained through SILAR method using 0.075 M anionic precursor, which lies on the hot surface of the Peltier element

Fig. 7 a—Infrared transmittance spectra for FTO substrate and for three CuI/FTO samples with different CuI thicknesses t, which were deposited on FTO substrates via 40 cycles of SILAR using different concentrations of anionic precursor NaI; **b**—FTIR spectra of the KBr supported CuI tablets obtained by scraping copper iodide from these samples
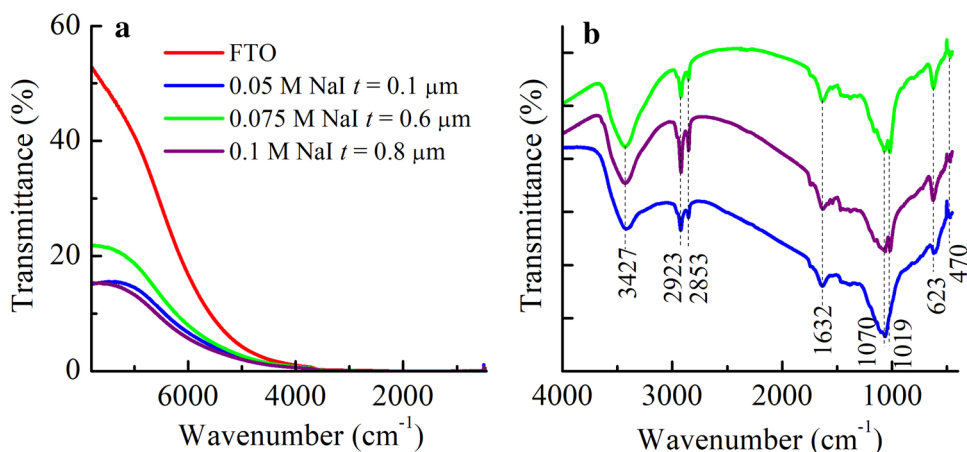
tetrathionate ions $S_4O_6^{2-}$. The presence of sulfate ions is connected with the use of copper sulfate in the cationic precursor, and tetrathionate ion is formed in the cationic precursor, where the Cu^{2+} ions in the presence of sodium thiosulphate are reduced to Cu^+ ions according to the following equation:

$$2CuSO_4 + 3Na_2S_2O_3 \rightarrow Cu_2S_2O_3 + 2Na_2SO_4 + Na_2S_4O_6 \tag{5}$$
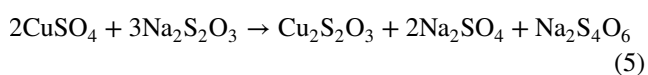
The Cu^+-ions form soluble complexes with the thiosulfate ions in the cationic precursor according to the following reaction:

$$Cu_2S_2O_3 + Na_2S_2O_3 \rightarrow 2Na[Cu(S_2O_3)] \tag{6}$$
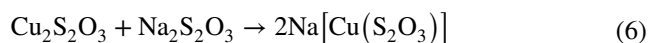
This complex along with ions Cu^+, SO_4^{2-} and $S_4O_6^{2-}$ can be firmly adsorbed on the substrate and on the CuI film surface, not being removed when washed in distilled water, and

then can react in the anionic precursor with sodium iodide to form CuI as follows:

$$2Na\left[Cu\left(S_2O_3\right)\right] + 2NaI \rightarrow 2CuI \downarrow + 2Na_2S_2O_3 \qquad (7)$$

The above interpretation is confirmed by the XRF data on the presence of sulfur in the CuI films.

The peak at ~ 1600 cm^{-1} can also correspond to C=O vibration of gaseous molecules adsorbed on the CuI surface [25–27], and peaks at ~ 1020–1070 cm^{-1} may additionally refer to C–O bond [26] or C–H bond [27]. So, as seen in Fig. 7b, mid-infrared radiation is absorbed by CuI surface mostly because it is coated with organic and inorganic species. In this way, there is an important conclusion from our FTIR investigations, which is associated with a high adsorption capacity of the CuI films obtained via SILAR method due to their large specific surface. When water and other organic and inorganic species on the CuI surface absorb infrared radiation, this causes the energy increase through an exciting of O–H stretching and other vibrations. The above effect can manifest itself in a greater heating of CuI film in CuI/FTO samples compared to uncoated FTO. We observed a similar phenomenon in [9] as the greater heating of arrays of ZnO nanorods compared to uncoated FTO in ZnO/FTO sample ensuring its functioning as semi-transparent solar TENG. Note, that NIR radiation with $\lambda = 2.9$ μm (i.e., with wave number ~ 3435.6 cm^{-1}) has exactly such energy as the intense absorption peak in the FTIR spectra in Fig. 7b.

Further, we research output characteristics of the new design of vertical TENG test sample, which consisted of FTO plate partly covered by 0.6 μm thick CuI film, with banded Cr/Cu contacts shown in Fig. 1a. Figure 8 shows output voltage V_{out} and output power P_{out} versus output current I_{out} for TENG test sample on the base of CuI/FTO under heating up to 50 °C by means its illumination from 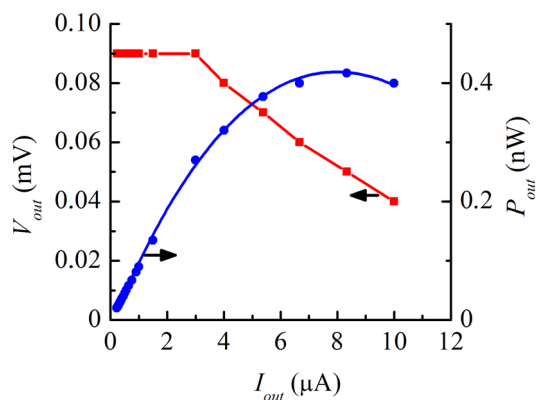the back side with the halogen lamp using setup presented in Fig. 1b. Before measurements of the output characteristics, the TENG test sample illuminated for half an hour, so that the device was completely warmed up. Figure 8 shows open circuit voltage $V_{oc} = 0.09$ mV and maximum output power $P_{max} = 0.4$ nW, when the whole test sample was submitted to a heat source and the average temperature of the TENG increased up to 50 °C. The obtained values correspond to those given for TENGs in [2, 3, 9]. A network of such thin-film nanogenerators by utilizing waste heat from environment may become a source of electricity sufficient, according to [2, 13], for autonomous operation of sensors.

Further, we found out that the design of the vertical TENG developed by us can be successfully used as the photoconductor type photosensor with composition Cu/Cr/CuI/FTO/Cr/Cu, due to the semiconductor CuI film and to the ohmic character of Cr/Cu contacts with both CuI and FTO. Figure 9 shows results of study the photosensitivity to ultraviolet and visible light for two test samples created on the base of the CuI films deposited on FTO substrates via SILAR. As it seen in Fig. 9, both test samples are the most sensitive to UV, due to the fact that the deposited via SILAR CuI films have a fairly wide band gap for direct optical transitions ($E_g \approx 2.9-3.0$ eV, according to Fig. 5). Along with this, the optical transitions caused by subband gap photons mainly due to the presence of point defects in the CuI, which was confirmed by large values of the Urbach energy in Fig. 5, explain the photosensitivity S of these films to visible light. Note, however, that S regularly decreases with increasing wavelength of light. The photocurrents I_{ph} recorded during illumination of the CuI/FTO test samples are large enough to not require amplification of the photosensor signal, the photoresponse time of the test samples $\tau_p \approx 30-100$ s, the reset time $\tau_r \approx 20-100$ s. As it seen in Fig. 9c, by the change of the SILAR mode for the deposition of CuI film, it is possible to control both the photosensitivity of the photosensor as a whole, and its selectivity with respect to the different light colors.

4 Conclusions

The researched in this work new design of vertical thermoelectric nanogenerator on the base of thin-film CuI/FTO composition with ohmic Cr/Cu contacts combines the functions of UV–Visible photosensor, that is, presents a two-function device. A distinctive feature of this device is its functioning as a TENG due to the spontaneous temperature gradient, which occurs at the uniform heating at the temperature range 303–323 K without a spatial temperature gradient in the environment. The explanation of the possibility of using CuI thin films produced by the SILAR method as both thermoelectric and photosensitive material turned out to be possible after studying their surface morphology, crystal structure,
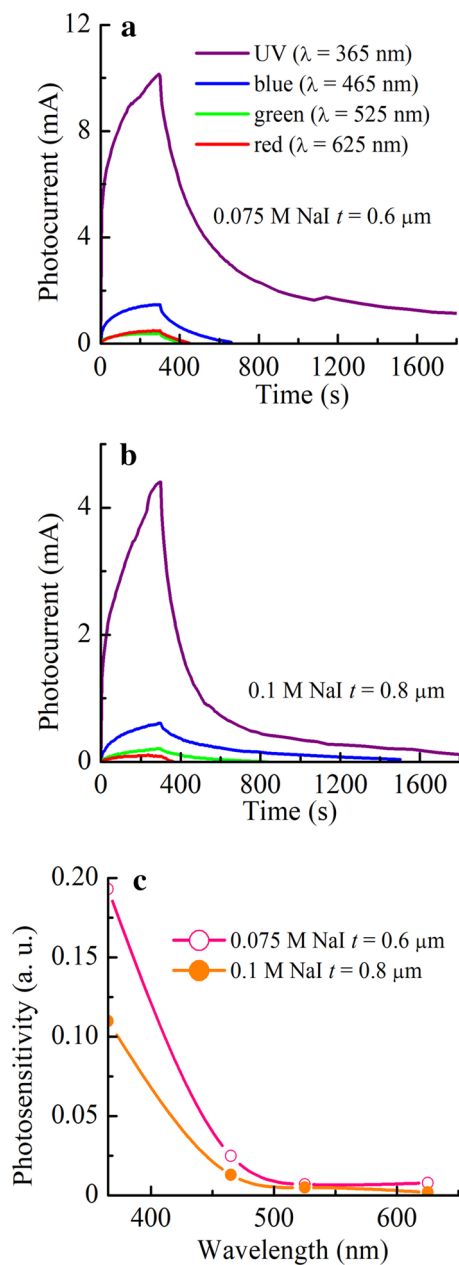
Fig. 8 Output voltage V_{out} (**a**) and output power P_{out} (**b**) versus output current I_{out} for TENG test sample on the base of CuI/FTO with 0.6 μm thick CuI film deposited via SILAR using 0.075 M NaI anionic precursor, at heating up to 50 °C by the halogen lamp

Fig. 9 Photoresponse curves measured at bias voltage 0.5 V under illumination by UV ($\lambda = 365$ nm), blue ($\lambda = 465$ nm), green ($\lambda = 525$ nm) or red ($\lambda = 625$ nm) light for two UV–Visible photosensor test samples having composition Cu/Cr/CuI/FTO/Cr/Cu with CuI films deposited via different SILAR modes: **a**—0.075 M NaI anionic precursor, $t = 0.6$ μm; **b**—0.1 M NaI anionic precursor, $t = 0.8$ μm. **c**—Photosensitivity S versus light wavelength λ for these test samples (Color figure online)

chemical composition and optical properties especially in the infrared range. It revealed that the obtained CuI films are wide-gap semiconductor material with many point defects caused optical transitions by subband gap photons. This generally provides the electrical conductivity and photosensitivity of the CuI films deposited on FTO substrates via

SILAR method to ultraviolet and visible light. The proposed design of UV–Visible photosensor possess high values of photocurrents I_{ph} under illumination trough FTO side, which eliminates necessity of amplification of the photosensor signal. The photoresponse and reset times of the photosensor are $\tau_p \approx 30$–100 s and $\tau_r \approx 20$–100 s, respectively. The large specific surface of the CuI films ensures favorable conditions for the adsorption of traces of the solutions from which CuI films were obtained by the SILAR method, and of gases and vapors from the atmosphere, in which infrared radiation, being absorbed, causes vibrations and stretching of molecular bonds that leads to the CuI heating. The created in this way temperature gradient approximately 7 K between CuI film and uncoated FTO substrate at total device temperature 30 °C ensures the functioning of the thin-film vertical TENG with Cu/Cr/CuI/FTO/Cr/Cu composition presented here. The output characteristics of the proposed design of the TENG provide the open circuit voltage $V_{oc} = 0.09$ mV and maximum output power $P_{max} = 0.4$ nW at temperature 50 °C.

Compliance with ethical standards

Conflicts of interest The authors declare that they have no conflicts of interest.

References

1. Y. Yang, K.C. Pradel, Q. Jing, J.M. Wu, F. Zhang, Y. Zhou, Y. Zhang, Z.L. Wang, ACS Nano **6**(8), 6984 (2012)
2. D. Tainoff, A. Proudhom, C. Tur, T. Crozes, S. Dufresnes, S. Dumont, D. Bourgault, O. Bourgeois, Nano Energy **57**, 804 (2019)
3. M. He, Y.-J. Lin, C.-M. Chiu, W. Yang, B. Zhang, D. Yun, Z.-H. Lin, Nano Energy **49**, 588 (2018)
4. M. Norouzi, M. Kolahdouz, P. Ebrahimi, M. Ganjian, R. Soleimanzadeh, K. Narimani, H. Radamson, Thin Solid Films **619**, 41 (2016)
5. T. Zhan, R. Yamato, S. Hashimoto, M. Tomita, S. Oba, Y. Himeda, K. Mesaki, H. Takezawa, R. Yokogawa, Y. Xu, T. Matsukawa, A. Ogura, Y. Kamakura, T. Watanabe, Sci. Technol. Adv. Mater. **19**(1), 443 (2018)
6. J.P. Rojas, D. Conchouso, A. Arevalo, D. Singh, I.G. Foulds, M.M. Hussain, Nano Energy **31**, 296 (2017)
7. Y. Xie, T.-M. Chou, W. Yang, M. He, Y. Zhao, N. Li, Z.-H. Lin, Semicond. Sci. Technol. **32**(4), 044003 (2017)
8. Y. Wu, S. Kuang, H. Li, H. Wang, R. Yang, Y. Zhai, G. Zhu, Z.L. Wang, Adv. Mater. Technol. **3**, 1800166 (2018)
9. N.P. Klochko, K.S. Klepikova, V.R. Kopach, I.I. Tyukhov, V.V. Starikov, D.S. Sofronov, I.V. Khrypunova, D.O. Zhadan, S.I. Petrushenko, S.V. Dukarov, V.M. Lyubov, M.V. Kirichenko, A.L. Khrypunova, Sol. Energy **184**, 230 (2019)
10. C. Yang, D. Souchay, M. Kneiß, M. Bogner, H.M. Wei, M. Lorenz, O. Oeckler, G. Benstetter, Y.Q. Fu, M. Grundmann, Nature Commun. **8**, 16076 (2017)

11. T. Ishibe, A. Tomeda, K. Watanabe, Y. Nakamura, IOP Conf. J. Phys. **1052**, 012126 (2018)
12. B.M.M. Faustino, D. Gomes, J. Faria, T. Juntunen, G. Gaspar, C. Bianchi, A. Almeida, A. Marques, I. Tittonen, I. Ferreira, Sci. Rep. **8**, 6867 (2018)
13. Y. Du, J. Xu, B. Paul, P. Eklund, Appl. Mater. Today **12**, 366 (2018)
14. B.N. Ezealigo, A.C. Nwanya, A. Simo, R.U. Osuji, R. Bucher, M. Maaza, F.I. Ezema, Arab. J. Chem. (2017). https://doi.org/10.1016/j.arabjc.2017.01.008
15. N.P. Klochko, V.R. Kopach, I.I. Tyukhov, G.S. Khrypunov, V.E. Korsun, V.O. Nikitin, V.M. Lyubov, M.V. Kirichenko, O.N. Otchenashko, D.O. Zhadan, M.O. Maslak, A.L. Khrypunova, Sol. Energy **157**, 657 (2017)
16. N.P. Klochko, K.S. Klepikova, V.R. Kopach, I.I. Tyukhov, D.O. Zhadan, G.S. Khrypunov, S.I. Petrushenko, S.V. Dukarov, V.M. Lyubov, M.V. Kirichenko, A.L. Khrypunova, Sol. Energy **171**, 704 (2018)
17. B.D. Viezbicke, S. Patel, B.E. Davis, D.P. Birnie, Phys. Status Solidi (B) **252**(8), 1700 (2015)
18. Amalina MN, Rusop M (2011) IEEE Student Conference on Research and Development. Cyberjaya, Malaysia. 10.1109/SCOReD.2011.6148761
19. M. Dongol, A. El-Denglawey, M.S. Abd El Sadek, I.S. Yahia, Optik **126**, 1352 (2015)
20. V.R. Kopach, K.S. Klepikova, N.P. Klochko, I.I. Tyukhov, G.S. Khrypunov, V.E. Korsun, V.M. Lyubov, A.V. Kopach, R.V. Zaitsev, M.V. Kirichenko, Sol. Energy **136**, 23 (2016)
21. S. Dhara, P.K. Giri, Rev. Nanosci. Nanotechnol. **2**(3), 1 (2013)
22. G. Lin, F. Zhao, Y. Zhao, D. Zhang, L. Yang, X. Xue, X. Wang, C. Qu, Q. Li, L. Zhang, Materials **9**, 990 (2016)
23. M. Kneiß, C. Yang, J. Barzola-Quiquia, G. Benndorf, H. von Wenckstern, P. Esquinazi, M. Lorenz, M. Grundmann, Adv. Mater. Interfaces **5**(6), 1701411 (2018)
24. M. Grundmann, F.-L. Schein, M. Lorenz, T. Böntgen, J. Lenzner, H. Wenckstern, Phys. Status Solidi A **210**, 1671 (2013)
25. T. Prakash, Adv. Mat. Lett. **2**(2), 131 (2011)
26. H.R. Humud, S. Hussein, Int. J. Chem.Tech. Res. **10**(9), 1109 (2017)
27. M.R. Johan, K. Si-Wen, N. Hawari, N.A.K. Aznan, Int. J. Electrochem. Sci. **7**, 4942 (2012)